Glacial Ring Forms on Axel Heiberg Island, Nunavut, Canada

Shannon M. Hibbard[1,2], Gordon R. Osinski[3], Etienne Godin[4], Chimira Andres[5], Antero Kukko[6,7], Shawn Chartrand[8], Anna Grau Galofre[9], A. Mark Jellinek[10], Wendy Boucher[11]

[1]Division of Earth and Ecosystem Sciences, Desert Research Institute, Reno, Nevada, 89512, USA
[2]Jet Propulsion Laboratory, California Institute of Technology, Pasadena, California, 91101, USA
[3]Department of Earth Sciences, University of Western Ontario, London, Ontario, N6A 5B7, Canada
[4]Centre d'Études Nordiques, Université Laval, Québec, Québec, Canada, G1V 0A6
[5]Lassonde School of Engineering, York University, Toronto, Ontario, M3J 1P3, Canada
[6]UNITE Flagship, Department of Remote Sensing and Photogrammetry, Finnish Geospatial Research Institute, Espoo, Finland
[7]Department of Built environment, Aalto University, Espoo, Finland
[8]School of Environmental Science, Simon Fraser University, Burnaby, British Columbia, V5A 1S6, Canada
[9]Laboratoire de Planétologie et Géosciences, CNRS UMR 6112, Nantes, France
[10]Department of Earth, Ocean and Atmospheric Sciences, University of British Columbia, V6T 1Z4, Canada
[11]School of Graduate Studies, Trent University, Peterborough, Ontario, K9L 0G2, Canada

Correspondence to: Shannon M. Hibbard (shannon.hibbard@dri.edu)

Abstract. Ring forms are a type of landform consisting of a series of ridges and troughs with a circular, sinuous, and anastomosing morphology. This striking landform was initially identified in the Canadian High Arctic on the south coast of Devon Island, Nunavut, Canada. Here, we report on the identification of ring forms near Mokka Fiord on Axel Heiberg Island, Nunavut, Canada. Utilizing field observations, ultra-high resolution LiDAR, and ground penetrating radar, we characterize and compare the morphometry and sedimentology of ring forms at Mokka Fiord with other similar periglacial, paraglacial, and glacial landforms. The Mokka Fiord ring forms range in diameter from 6 m to 37 m and reach up to 1.5 m in height and are composed of clast-rich glaciofluvial sediment and till. Based on both regional and local observations, results from nearby field investigations of glacial outwash plains on Axel Heiberg Island, and comparisons to other periglacial and glacial features sharing a similar morphology, we interpret Mokka Fiord ring forms as glacial in origin. Specifically, we propose Mokka Fiord ring forms are ice-marginal glaciofluvial kame terraces formed from the passive ablation of buried glacial ice, leading to the formation of hummocky ring forms. This formation mechanism supports a predominantly polythermal glacial environment with limited water supply throughout much of the Holocene.

1 Introduction

The Canadian High Arctic and has been subject to glacial and periglacial processes throughout the Quaternary Period. These processes can produce a wide variety of landforms, many of which are/were associated with massive ice. These landforms can often appear morphologically very similar and, thus, are difficult to differentiate. The Canadian High Arctic has only recently

undergone deglaciation and is, therefore, a predominantly paraglacial landscape that has experienced the effects of both recent glaciation and periglacial modification. Due to this and the remoteness of the area, it is challenging to differentiate between landforms (e.g., French and Harry, 1990). This has led to ongoing debate within the fields of periglacial and glacial geomorphology.

Much of the Canadian High Arctic lies in an environment favorable to polythermal and cold-based glaciers, which limits the glacial imprint on a landscape. Therefore, evidence of glaciation might be expected in the form of buried snout/ice-marginal glacial ice susceptible to glacial karst development, hummocky till veneers, glaciofluvial outwash, and kames (O' Cofaigh et al., 2003). However, periglacial processes can lead to hummocky terrain in till and glaciofluvial outwash sediments and produce epigenetic massive ice through ice segregation and injection (French and Harry, 1990), which is susceptible to thermokarst degradation. The topographic inversion of glacial sediments (e.g., Fairbridge, 1968; Thompson et al., 2016; Westoby et al., 2020) due to the ablation of underlying glacial ice is a common mechanism for the production of hummocky surfaces in deglaciated landscapes (e.g., Clayton, 1964; McKenzie, 1969; Embleton and King, 1975; Knudsen et al., 2006; Krüger et al., 2010; Moore, 2021). This process usually forms a series of landforms characterized by mounds and depressions following the retreat of a glacier and has been observed to create conspicuous circular (e.g., Gravenor and Kupsch, 1959) to sinuous and anastomosing (e.g., Knudsen et al., 2006; Hibbard et al., 2021) morainic ridges. Yet, the ablation of buried non-glacial ice can produce morphologically similar features (e.g., Mackay, 1974; Rampton, 1988; Mollard, 2000). Thus, the origin of such morphologically similar features is still a topic of debate (e.g., Watson and Watson, 1974; Ross et al., 2019).

Whereas these features may appear similar in the field, the processes by which they form are very different. Massive ground ice, in the form of both buried glacial ice and epigenetic segregation ice, is common across the Canadian High Arctic (O'Neill et al., 2019). Differentiating between massive ice origins and the associated landform origins is key to understanding the evolution of high arctic landscapes and reconstructing Quaternary environmental conditions. This is especially true in the continuous permafrost zones, where the presence of massive segregation ice and periglacial landforms can inform us about climate evolution during deglaciation and the effects climate change has in high arctic environments.

Here, we report on an undocumented landform on the east coast of Axel Heiberg Island near Mokka Fiord in Nunavut, Canada, that appears remarkably similar to ring forms recently identified at Dundas Harbour on Tallurutit (Devon Island) (Hibbard et al., 2021). Ring forms (a general non-genetic term established by Johnson and Clayton (2003) and used to encompass the variety of naming schemes used in the literature) are circular to anastomosing raised-ridge features that can be of periglacial or glacial origin. We provide a comparison of Mokka Fiord ring form morphometrics, substrate characteristics, and associated landforms and processes, to other morphologically similar glacial and periglacial landforms and present a working hypothesis for the formation of this landform and the implications it has on past climate conditions during the Holocene.

2 Geologic and Geomorphic Setting

Axel Heiberg Island (Umingmat Nunaat) in the Qikiqtani region of Nunavut of Inuit Nunangat in Canada (Fig. 1) is a part of the Sverdrup Islands in the Queen Elizabeth Islands of the Canadian Arctic Archipelago. Axel Heiberg Island lies within the Sverdrup Basin which is the thickest section measuring up to 13 km, and is predominantly composed of Carboniferous to Paleogene siliciclastics, evaporites, and carbonates (Balkwill, 1978; Russell et al., 2006; Embry and Beauchamp, 2008; Harrison and Jackson, 2014). Quaternary deposits, including stream, deltaic, glacial, and marine beach sediments, were deposited over bedrock geology and occupy valley floors and raised beach sediments along the coasts (Thorsteinsson, 1971a, 1971b).

The island hosts two major ice caps, the Müller Ice Cap and Steacie Ice Cap (Fig. 1a), and a wide range of glacier types such as cirque, outlet, piedmont, and valley glaciers (Ommanney, 1969; Thomson et al., 2011). The thermal regime of glaciers presently on Axel Heiberg Island are cold and polythermal (Blatter, 1987; Ó Cofaigh et al., 1999) which is thought to have extended into the last glacial maximum with the exception of fjord glaciers interpreted to be warm-based glaciers and ice streams (Ó Cofaigh et al., 1999; England et al., 2006). Axel Heiberg Island was covered by the Innuitian Ice Sheet, which reached its last glacial maximum around 29 ka BP (Bednarski, 1998). Extensive deglaciation of the Innuitian Ice Sheet occurred predominantly from west to east from 16.5–11 ka BP and marine-based ice largely disappeared by 9 ka BP leaving mostly land-based ice on Axel Heiberg and other islands (England et al., 2006). Deglaciation of the island pursued and freed most of its fjords of ice by 8 ka BP (England et al., 2006) until reaching contemporary conditions around 7.5 ka BP. The marine limit varies across Axel Heiberg Island but has been reported to range between 78 and 158 m asl today (e.g., Bednarski, 1998; Pollard and Bell, 1998; Dyke et al., 2005).

Our field of study (Fig. 1b) lies within the Granite dispersal train (Ó Cofaigh et al., 2000; England et al., 2006) and is composed of Quaternary deposits (Thorsteinsson, 1971a, 1971b). Detailed surveying of ring forms was conducted at one main field site located on a terrace along a channel trending northwest-southeast feeding into Mokka Fiord. Bednarski (1998) surveyed the coast of Nansen Sound and Flat Sound ~300 km to the northwest and identified an area dominated by meltwater channels sourced from the western highlands, moraines and kame terraces, and marine sediments. However, to our knowledge, surficial geology and geomorphology of our field site have not been directly studied.

Present-day conditions represent a polar desert environment (Andersen et al., 2002). The nearest long-term climate station is Eureka A located on the coast of Fosheim Peninsula on Mirnguiqsirvik (Ellesmere Island) ~ 300 km northeast of the field site. The Canadian Climate Normals Eureka A station data for 1981–2010 shows mean annual air temperature of −18.8°C, mean annual precipitation of 79.1 mm, and mean annual snowfall of 60.3 cm (Environment Canada, 2021). Permafrost thickness has been estimated to be 400–600 m at Mokka Fiord (Taylor and Judge, 1976; Pollard et al., 1999). While the average climate

100 suggests a polar desert, the Arctic experiences some of the most intense summertime climate variability leading to wet precipitation and glacial/snow melting events (Constable et al., 2022) which contrasts sharply with typical polar desert conditions.
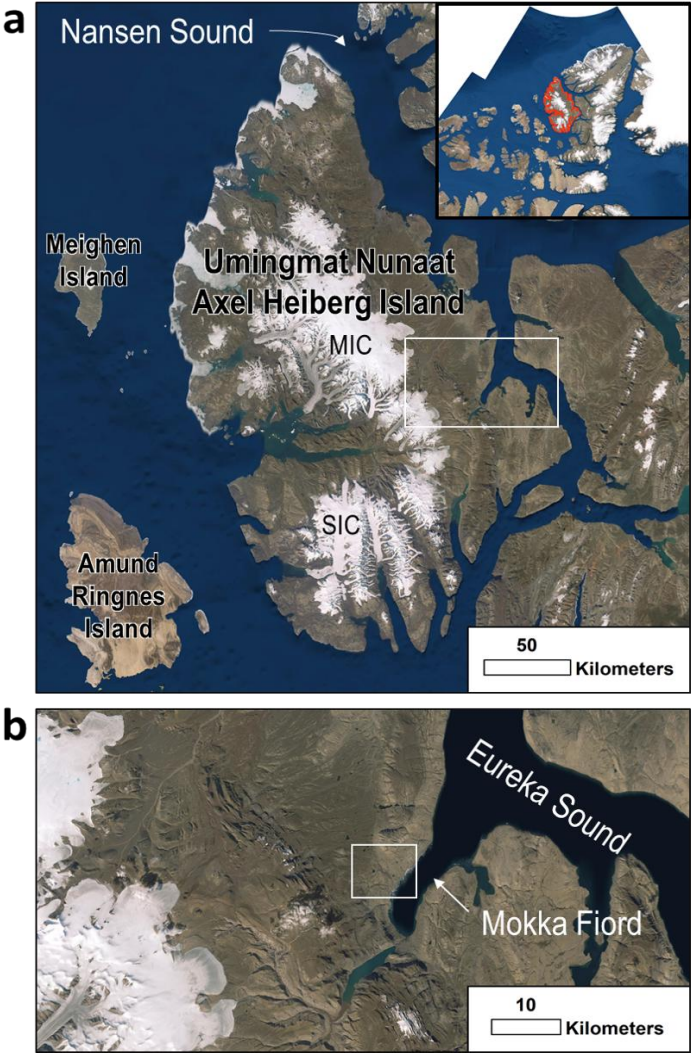
Figure 1: Axel Heiberg Island observed using World Imagery (Esri, 2018). (a) Axel Heiberg Island is located in Nunavut, Canada
105 **and is outlined in red in top right map inset. Nansen Sound runs along the east coast of much of Axel Heiberg Island. White box locates panel b. MIC and SIC represent Müller Ice Cap and Steacie Ice Cap, respectively. (b) Location of the field region (located within white box centered at 79.61589, -87.5556) is northeast of Mokka Fiord, which feeds into Eureka Sound. World Imagery Source: Esri, Maxar, GeoEye, Earthstar Geographics, CNES/Airbus DS, USDA, USGS, AeroGRID, IGN, and the GIS User Community.**

3. Methodology

Fieldwork was carried out ~4 km northwest of Mokka Fiord on Axel Heiberg Island in July 2019 (Fig. 1). Field reconnaissance was done on foot and by helicopter. This led to the identification of ring forms across multiple terraces along one river channel that feeds Mokka Fiord. A terrace along the channel was selected for in-depth field analysis. To characterize the landform, we employed trenching to observe grain size differences in ridges versus troughs and to identify preferential orientations, along with Light Detection and Ranging (LiDAR) and Ground Penetrating Radar (GPR).

AkhkaR4DW, a backpack mobile laser scanning system was used to kinematically collect high-precision 3D topographic data (Kukko et al., 2012; Liang et al., 2015; Kukko et al., 2017, 2020; Hyyppä et al., 2020). This system was developed by the Finnish Geospatial Research Institute to produce ultra-high resolution digital elevation models (DEMs) at 1–5 cm scale. The positioning of the system relies on post-processed tightly coupled differential processing of data from a GNSS receiver (NovAtel Pwrpak7) observing GPS and GLONASS satellite constellations and an inertial measurement unit (GNSS-IMU, NovAtel ISA-100C) (Kukko et al., 2020).

The LiDAR point cloud LAS file was produced using RiProcess and TerraScan software to filter and reduce the raw point cloud data which had a total of 46,163,219 points covering an area of ~6.42 ha with an average density of 164.2 points/m^2. WhiteBox Geospatial Analysis ToolBox (GAT), an open-source geospatial data analysis software developed by Professor John Lindsay at the University of Guelph (Lindsay, 2014, 2016), was used to create a Bare Earth DEM and Hillshade. The Bare Earth DEM was created using an inverse-distance weighting (IDW) scheme. A search distance of 10 cm was used to interpolate the point cloud. The Power (p) exponent was set to the default value of 2. Points that exceeded a slope of 30° from the unmeasured point being calculated were considered an outlier/non-ground point and were not used in the output point-cloud. A grid resolution of 5 cm/pixel was used to provide a high-resolution DEM with reasonably short processing time. The Hillshade azimuth (direction of the sun), measured clockwise from North, was set NW to 315°. The altitude, or angle of illumination, measured from the horizon to normal, was set to 30°. The Bare Earth DEM and Hillshade files were loaded into Esri's ArcGIS Desktop 10.8.1 using the World Geodetic System reference coordinate system and the Universal Transverse Mercator projection in zone 16N (WGS 1984 UTM 16N).

A Sensors and Software 250 NOGGIN SmartTow GPR system was used to investigate massive ice and deposit thickness; the instrument was equipped with a 250 MHz antenna. Three GPR lines were collected, three of which lie within the LiDAR data, ranging from 20–30 m in length. Signal velocity was determined based on sedimentology, diffraction hyperbola fitting, and context from trenching in the field, which was determined to be 0.125 m/ns (frozen and unfrozen sand and gravel). Based on this signal velocity, GPR signals penetrated down to roughly 4 m before heavily attenuating. GPR data was collected on July 8, 2019, therefore, the thaw depth is representative of that day of the year, which was measured/estimated at 1–1.5 m.

GPR data was analyzed using Sensors and Software's Ekko_Project_5 software. GPR data was dewowed and was amplified with a Spherical Exponential Calibrated Compensation (SEC2) gain and an Attenuation value of 8. Elevation data along each GPR line was extracted from the LiDAR dataset and added to the GPR data file. This corrects for unreliable depths of key subsurface features, but slightly stretches the upper part of the cross-section image.

4 Observations and Results

4.1 Context and Setting of Mokka Fiord Ring Forms

We identified ring forms on seven terraces along a northwest-southeast trending meltwater channel flowing into Mokka Fiord (Figs. 2–4, and S1, Supp. files), five of which are located on the western side of the channel and two on the eastern side. The terraces occur at different elevations, with the uppermost terrace occurring at an average elevation of 166 m on the west side, and the lowermost terrace occurring at 114 m on the east side. An additional five ring form sites were identified up and down valley from the investigated terraces by helicopter (Figs. 2 and 3), one of which was located in the floodplain of the stream system (Fig. 3e). Ring forms were also observed near Strand Fiord (Fig. 3g) suggesting these features are not unique to Mokka Fiord.

The ring forms at Mokka Fiord occur in three surficial geologic units mapped by the Geological Survey of Canada (2022), including (1) terraced sediments (At), comprised of coarse surface sediments and patterned ground, (2) till, morainal sediments, undifferentiated (T.W) comprised of marine reworked glacial diamicton, and (3) colluvial deposits, undifferentiated (C.W) comprised of a heterogeneous mixture of source rocks and grain sizes that are products of mass waste and have patterned ground. Our field observations support these regional interpretations and indicate that all ring forms occur in coarse-grained diamicton that is glacially or glaciofluvially sourced.

Polygonally patterned ground and solifluction were observed in proximity to the field sites. Ponds of water (Fig. 3e), wet soil (Figs. 3c, d), and thaw slumps (not seen in the 2011 Maxar image (Fig. 2) of the World Imagery data) (Fig. 4) were also observed at many of the ring form sites indicating the presence of ice-rich permafrost undergoing active thermokarst degradation.

170

Figure 2: Maxar (WV02) image of the field region at Mokka Fiord in World Imagery taken in 2011 (Esri, 2018). Seven terraces containing ring forms are outlined in white. Average elevation (in meters) of each terrace is numbered in white. White dots indicate figure locations with figure numbers labelled in white. White arrow points to the location of the riverbank in Figure 7a. Elevation contours are labelled every 50 m and obtained from ArcticDEM Release 7 (Porter et al., 2018). The asterisked elevation denotes the main field site for in-depth field analysis (i.e., GPR, LiDAR, and trenching). World Imagery Source: Esri, Maxar, GeoEye, Earthstar Geographics, CNES/Airbus DS, USDA, USGS, AeroGRID, IGN, and the GIS User Community.

4.2 Morphologic Description of Mokka Fiord Ring Forms

Ring forms found across the field region (Fig. 2) exhibit a circular, elongate, sinuous and/or anastomosing ridge and trough morphology in planform (Figs. 3 and 5). Ring forms can exhibit individual closed cells (i.e., ridges forming a closed loop encircling a central trough) that are circular (Figs. 3b, e, and 5), semi-circular (Figs. 3a, b, c, e, and 5) or elongated (Figs. 3c, f, and 5). Ring forms range from being closely spaced and interconnected (Figs. 3a, b, d, g) to well-spaced and isolated (Fig. 3e), or somewhere in between (Figs. 3c, f, and 5). Minimal vegetation is found in the field region but can act as a distinguishing factor between the ridges and their surroundings (Figs. 3 and 5b).

One terrace was surveyed in detail (referred to as the main field site) to further investigate the ring forms (Figs. 2 and 5). Ring forms at this site have raised convex ridges that stand above the rest of the surrounding deposit and frequently encircle a central concave depression thus forming individual closed cells (Fig. 5). Ridges are also subdued, shallow and wide relative to the more prominent narrow convex ridges (Fig. 5). Small sharp-crested conical mounds (Fig. 3d) and rounded mounds (Fig. S1a,b, Supp. Files) are found in the same deposit as the ring forms. Terrain adjacent to the ridges and closed cells is referred to as "mesh" which is the part of the deposit that interconnects ring forms and acts as the baseline of the deposit (Fig. 6). The central depressions of closed-cell ring forms lie at the same elevation at or higher than the mesh with ridges elevated above their adjacent terrain (Figs. 5 and 6). Topographic profiles (Fig. 6) of the ring forms show this mesh-ridge-trough sequence. The topographic lows (i.e., mesh and central depressions) at the main field site are poorly drained and host grasses and mosses (Fig. S1c, d, Supp. Files) compared to the dryer ridges that host lichen (Fig. S2, Supp. Files). A thin white salt crust can also be found across the ring form materials (i.e., the materials of which the ridges, troughs and mesh are composed) (Fig. 5a) generally found resting at the base of the ridges or in topographic lows.

The ring form materials at the main field site are cut by a stream exposing a ~6 m thick cliff that transitions into a ~12 m thick gentler sloping lobate material before connecting with the riverbed (Figs. 2 and 7a), suggesting the deposit has a minimum thickness of ~6 m at the river cutbank relative elevation. The lobate slumping of the lower ~12 m of material is interpreted to be the result of solifluction linked to ice-rich permafrost. A pit was dug 89 cm into the mesh of the deposit without reaching the thaw depth (July 2019) (Fig. 7b). The deposit (observed at the cutbank and in the pit) is a gravelly diamicton composed of poorly sorted, clast-rich, sub-rounded to rounded silt, sand, pebbles and cobbles with minor evidence for a preferred flat orientation of large grains (Fig. 7b). Fewer cobbles were present below 70 cm in the pit. Small pits (~10 cm deep) were also dug in a ridge and central trough of a closed-cell ring form. No grain sorting was observed. Fabrics and grain size analyses were not done due to helicopter time constraints at the field site.

Ridges can reach up to 1.5 m in height when measured from the ridge apex to the adjacent low-lying terrain (i.e., mesh); although most do not exceed 1 m in height (Figs. 5 and 6). Closed-cell ridges (i.e., ridges that enclose a central depression) range in height from 0.2–0.6 m when measured from the lowest point in the central trough to the highest point on the ridge (Fig. 6). Ridge width ranges from 1.5–9 m but more commonly ranges from 3–4 m from the outer edges of the ridge (Fig. 5).
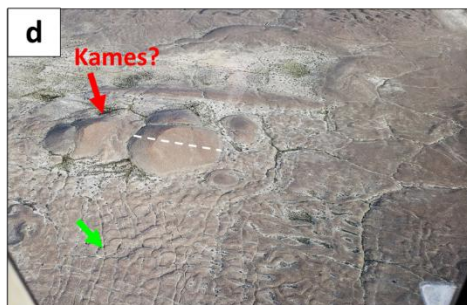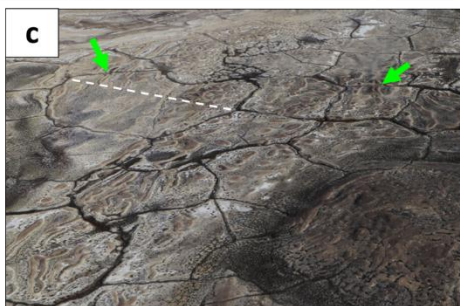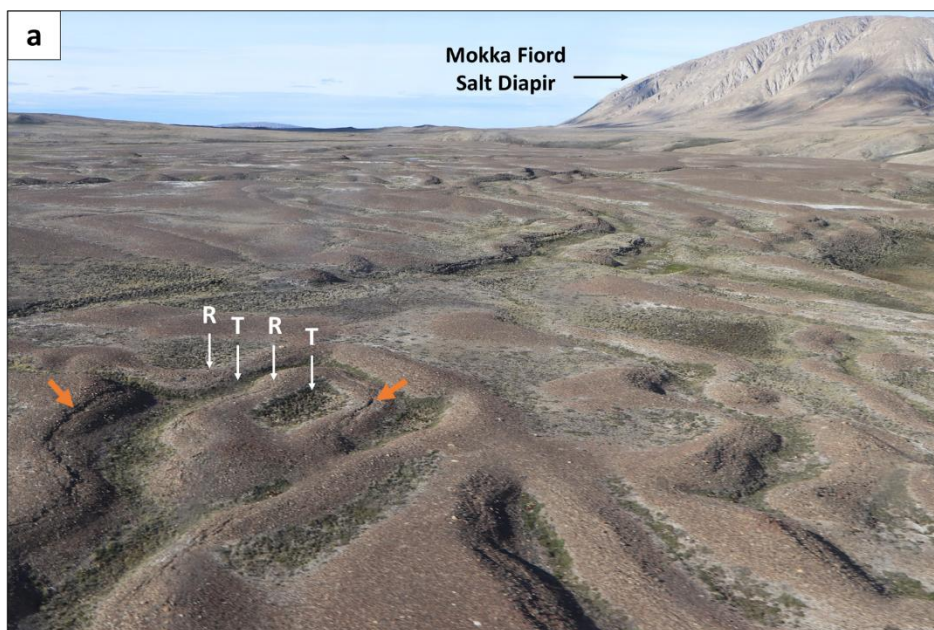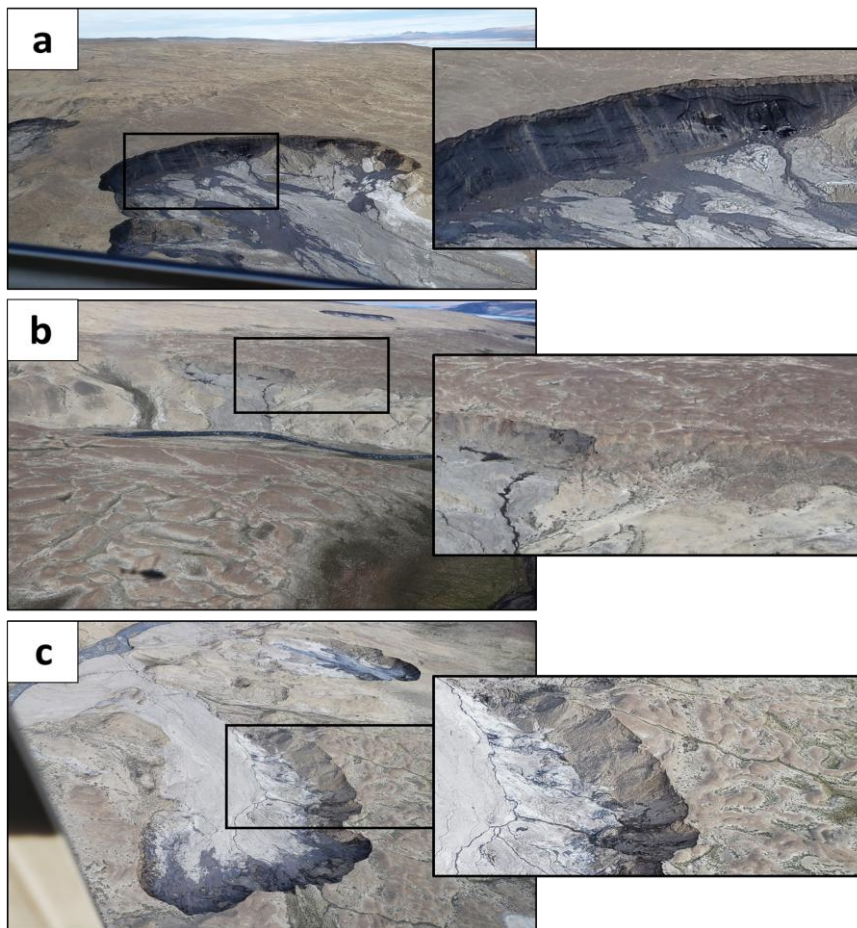
Figure 4: Thaw slumps in the field region. Figure locations can be found in Figure 2 by white dots. (a) West side of channel, south of field site. Massive ice exposed at thaw slump. Thaw slump exposure is 10−15 m thick, including ~1−2 m of dry material above wet material. Deformed massive ice underlying overburden with an undisturbed contact. (b) East side of the channel, directly opposite

the field site. A brown deposit with ring forms overlies a lighter-toned deposit. Overlying deposit thickness is ~10−15 m. (c) West side of channel, south of field site. Deposit with sinuous and anastomosing ring forms overlying lighter-toned sediments. Deposit thickness is ~10−15 m. Two active thaw slumps visible in image.

230 Thirty-two closed-cell ring forms with central troughs were mapped in the LiDAR area. The long axis of closed-cell ridges ranges from 5.8–36.8 m with an average of 15.8 m. The orientation of the long axes (north = 0°) range between 1.8° and 174.5° with an average of 95.7°. This orientation is near perpendicular to the roughly north-south running channel hosting the terraces (Fig. 2). The short axis of closed-cell ridges ranges from 4.3–12 m with an average of 8.2 m.

235 Cracks were found running along or just off-center from the axial trace of many ridges (Figs. 3a and S2, Supp. Files), and closed-cell ridges generally have a crack running off-center from the axial trace along the inner part of the cell (Fig. S2a, Supp. Files). Cracks present themselves as a thin and narrow cavity along the ridge (Figs. 6 and S2, Supp. Files), and slumping of the surrounding material may be present. Cracking also occurs along the center of polygon troughs and along the shoulders of polygons (Fig. S2c, Supp. Files), both of which tend to be much wider (≤ 30 cm) and deeper than the cracks observed on the

240 ridges of ring forms.
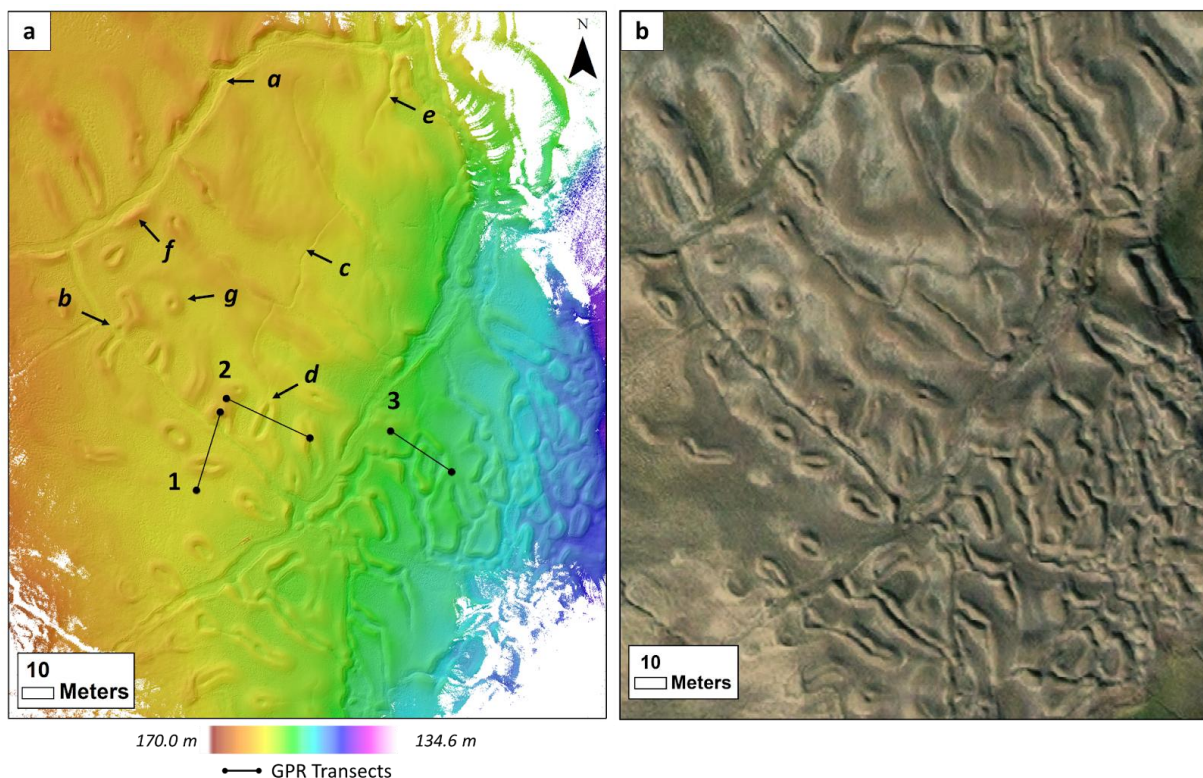
Figure 5: Digital Elevation Model (DEM) of ring forms at the main field site. (a) DEM is overlying hillshade with 315° azimuth. GPR transects 1–3 are numbered and outlined in black. Topographic profiles and GPR transects can be found in Figure 6. Features of note include: a - shallow and wide raised ridges cross-cut by polygon trough, b - closed-cell ring form cross-cut by polygon trough, c - secondary trough cross-cutting ring form, d - secondary trough cuts down through the middle of a closed-cell ring form, e - secondary trough runs down the middle of a shallow sinuous ring form, f - raised polygon shoulder, g - perfectly circular individual closed-cell ring form. (b) Main field site LiDAR area in World Imagery (Esri, 2018). World Imagery Source: Esri, Maxar, GeoEye, Earthstar Geographics, CNES/Airbus DS, USDA, USGS, AeroGRID, IGN, and the GIS User Community.

245

250

255 **Yellow dashed line in GPR transects represents thaw depth (i.e., depth to permafrost in July 2019). Thaw depth generally follows topography but is not a continuous thickness. Red arrows along GPR transect indicate location of massive ice beneath the thaw depth. Stacked alternating black and white reflectors can be seen beneath many closed cell ring form central troughs indicating the presence of an ice wedge. Ice lenses or proto wedges are common beneath ridge cracks.**

260 Polygons are also present at the main field site. Polygons range in diameter (long axis) from 63–167 m, and trough width averages around 3 m, but can reach up to nearly 6 m. Thin and narrow secondary troughs are present within the larger polygon centers (Fig. 5). Secondary troughs extend from a primary trough and often terminate within the polygon center (Fig. 5). Polygon troughs typically cross-cut ring forms but can also merge with the ring forms to create an anastomosing ensemble of ridges and troughs (Figs. 3 and 5).

265

Ring form morphology varies laterally and with elevation among the terraces. The main field site is characterized by more mounds down-valley (Fig. S1a, Supp. Files) and less mounds with high-center polygons exposing the same deposit hosting the ring forms up-valley (Fig. S1d, Supp. Files). Additionally, the uppermost terrace has a thin deposit that appears degraded (i.e., subtle hummocks, thin deposit, less pronounced morphology) with subdued ring forms (Fig. S1e, Supp. Files) relative to
270 ring forms on neighboring, lower terraces that appear to reside in much thicker deposits (Fig. S1b,f, Supp. Files). Additionally, more vegetation is present at the main field site (Fig. S1c,d, Supp. Files) compared to the other terraces (e.g., Fig. S1a,b,e,f, Supp. Files).
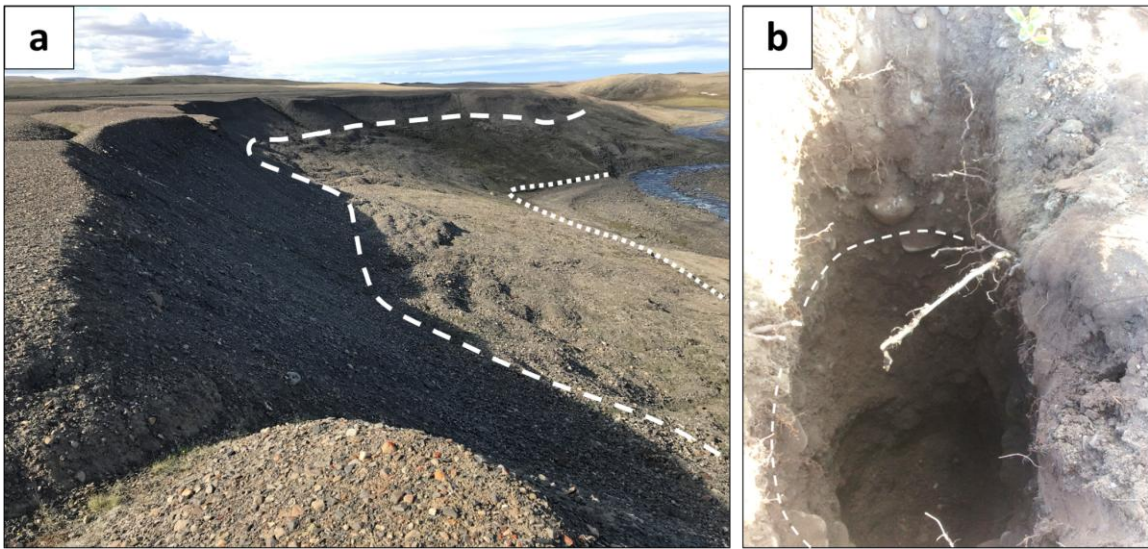
Figure 7: Characteristics of ring form materials at river cutbank. (a) River cutbank exposing deposit thickness (Location identified
275 **in Figure 2). Polygons are visible at the top of the deposit. The surface to the white dashed line is characterized by a steep talus slope ~ 6 m thick. A gently sloped ~12 m section of lobate material occurs between the white dashed line and the white dotted line and is**

interpreted to be the result of solifluction. Below the white dotted line is a river sand bank. (b) Pit dug 89 cm into the main field terrace. White dashed line outlines flat-oriented gravel.

280   Three GPR transects were collected at the main field site. Lines 1, 2, and 3 cross over closed-cell ring forms (Figs. 5 and 6) and show a thaw depth (July 2019) from 1–1.5 m that can be identified by a nearly continuous bright linear reflection below the surface (Fig. 6). Stacked bright radar reflections are observed below the central depression of a closed-cell ridge at Lines 1 and 2 (Fig. 6). Line 3 shows bright reflections beneath two troughs adjacent to a closed-cell ridge. However, the center of the closed-cell ridge at Line 3 does not appear to have an obvious bright reflection. Deposit thickness is indeterminate in the

285   GPR transects, suggesting the deposit thickness exceeds the signal penetration depth of approximately 4 m. Ring forms were also observed directly on top of thaw slumps across the field region, which exposed deposits as thick as 10–15 m.

5 Discussion

We have documented ring forms northwest of Mokka Fiord on Axel Heiberg Island, Nunavut, Canada. These features exhibit a circular, elongated, sinuous, and/or anastomosing series of ridges and troughs (Figs. 3 and 5) and are near-identical to features

290   documented on the south coast of Devon Island (Hibbard et al., 2021). Below, we compare ring forms on Axel Heiberg Island to other morphologically similar periglacial and glacial landforms to better elucidate an origin (Table 1).

5.1 Periglacial Origins

Patterned ground is a common product of periglacial processes that can result in conspicuous morphologies such as circular,

295   sinuous, and anastomosing ridges and troughs. Stone circles are a common periglacial feature that exhibit this morphology and can be found in high and low arctic regions (Washburn, 1956; Schmertmann and Taylor, 1965; Washburn, 1973; Hallet and Prestrud, 1986; Hallet, 2013). Stone circles are characterized by their circular to labyrinthine coarse-grained ridges surrounding a central fine-grained domain. Ridge width typically ranges from 0.5–1 m and ridge height usually reaches up to 0.5 m, with circle diameters ranging from 2–5 m (Hallet and Prestrud, 1986; Kessler et al., 2001; Hallet, 2013). Stone circles also

300   commonly exhibit cracks along the axial trace of circular ridges that form from frost heave and soil upwelling (Kääb et al., 2014), similar to what is observed at Mokka Fiord (Figs. 3 and 6). However, while the scale is similar, no grain sorting or evidence of soil upwelling was observed in the Mokka Fiord ring forms and the microtopography does not reflect that of stone circles. Thus, the properties of the Mokka Fiord ring forms are inconsistent with a stone circle origin.

305   Collapsed pingos, palsas, lithalsas, or other frost mounds (Table 1), also referred to as circular ramparts or ramparted depressions, are periglacial landforms that can also result in circular raised ridge features (Table 1) (Mackay, 1998 and references therein). Pingos are perennial ice-cored hills produced by injection of groundwater under artesian pressure (Holmes

et al., 1968; Müller, 1962) or by pore-water expulsion resulting from permafrost aggradation in a water-saturated sandy sediment, such as a shallow lake (Mackay, 1998). Sources of water for pingo formation in arctic environments include the outflow of perennial subpermafrost springs in Svalbard (Demidov et al., 2022), possible sub and intra permafrost water flow from nival and/or buried ice melt in Greenland (Allen et al., 1976), glacial meltwater recharge, or deep groundwater injection (Henkemans, 2016). However, pingos are much larger in scale, typically occur singularly, and are associated with high local relief (open-system pingos) or drained lake basins (closed-system pingos) (Table 1) and, therefore, are not comparable to the ring forms at Mokka Fiord.

315

Table 1: Periglacial and glacial ring ridge feature morphometrics compared to Mokka Fjord VRFs. Modified from Hibbard et al. (2021).

Lithalsas are smaller scale frost mounds that form by ice segregation in mineral-rich soil absent of peat and can be found on river terraces and along streams. They form through permafrost aggradation causing localized ice segregation as pore water migrates (Calmels et al., 2008). The formation of lithalsas requires specific environmental conditions related to slow freezing times to promote cryosuction for ice lens growth. The limited examples of contemporary lithalsas appear to be restricted to the discontinuous permafrost zone with available groundwater supply and in frost susceptible fine-grained sediment as opposed to the coarser grained sediments like what we observe in our study area (Calmels et al., 2008; Wolfe et al., 2014); although others have proposed lithalsa remnants to be present in coarse-grained materials (e.g., Rapp and Rudberg, 1960; Seppala, 1972; Akerman and Malmstrom, 1986; Coxen, 1986; Hosek et al., 2019). Lithalsas are argued to develop in areas where water is abundantly available and not limited to a shallow active layer (Pissart, 2002) as would be expected in the continuous permafrost zone found at Mokka Fiord. It is argued that only seasonal or short-lived frost mounds and blisters could form in the continuous permafrost zone due to limited hydrostatic conditions (French, 1971; Morse and Burn, 2014).

However, Paquette et al. (2020) argued that small lithalsa plateaus formed in the High Arctic near Resolute Bay on Cornwallis Island, Nunavut, Canada in a shallow wetland. They suggest the formation of ice lenses can slowly heave the wetlands upwards, eventually exposing water-saturated materials to air temperatures leading to additional permafrost aggradation and ice lens formation. To the authors knowledge, this is a unique example of a possible contemporary high arctic lithalsa that Paquette et al. (2020) argue is only possible due to the sustained water supply provided by the wetland setting. Mokka Fiord ring forms reside in a floodplain which may have experienced occasional flooding through the Holocene climate. Yet, this would not provide the sustained water supply that a wetland provides. The necessity for warm permafrost conditions, slow freezing rates, and abundant water supply that can migrate upward to the freezing front for lithalsa formation make Mokka Fiord ring forms an unlikely candidate. Mokka Fiord ring forms are located in the continuous permafrost zone characterized by a cold permafrost environment that would not have promoted lithalsa development (Wolfe et al., 2014). Additionally, ring forms at Mokka Fiord exhibit a much more complex morphology than has been observed in remnant and contemporary lithalsas (Fig. 3), which tend to be circular ramparts.

Other segregation ice landforms display more similar morphologies to Mokka Fiord ring forms. The Involuted Hill sites located in Tuktoyaktuk, Northwest Territories, Canada, are clay till-mantled ice-cored hills with a series of ridges and troughs and exhibit a similar, yet not identical, complex morphology as observed in Mokka Fiord ring forms. The ridges there are approximately 10–40 m wide, several tens of meters in length, and up to 6 m in height (Mackay, 1963; Rampton, 1988; Mackay and Dallimore, 1992). Mackay and Dallimore (1992) suggest glacial meltwater and porewater expulsion are what led to the formation of the massive ice at Involuted Hill, and that differential degradation of that ice led to the series of ridges and troughs at the surface. This landform is found at lower latitudes, providing more opportunity for talik formation and permafrost aggradation than at Mokka Fiord. Yet, smaller pingo-like frost mounds and partially collapsed mounds have been documented in the Canadian High Arctic on Banks Island, Northwest Territories. These are suggested to form from the freezing of fluvial

taliks left over from previous lateral stream migration (Pissart and French, 1976, 1977). Furthermore, pingos in Svalbard have been suggested to form from the infiltration and migration of polythermal glacial meltwater to taliks (Liestøl, 1977). However, these are isolated frost mounds, unlike what is observed at Mokka Fiord. Additionally, taliks typically form beneath deep bodies of water (~1.5–4 m) such as lakes or large rivers (Mackay et al., 1998; Burn, 2002; Jorgenson and Shur, 2007; Arp et al., 2011) unlike what is observed at Mokka Fiord.

These examples of frost mounds demonstrate the diversity of environmental conditions, water availability, and morphology/morphometry observed across ice segregation features. The thermal regime of glaciers on Axel Heiberg Island today are cold and polythermal (Blatter, 1987; Ó Cofaigh et al., 1999) which is thought to have extended into the last glacial maximum, except for fjord glaciers, which are interpreted to be warm-based glaciers, and ice streams (England et al., 2006; Ó Cofaigh et al., 1999). There is minimal evidence of wet-based glaciation on the island, with only minor evidence of striated bedrock and erratic dispersal trains resulting from localized warm-based conditions (Ó Cofaigh et al., 1999), supporting a largely polythermal/cold thermal regime. Segregated ground ice is typically associated with postglacial permafrost aggradation in glaciolacustrine fine-grained tills, or in more recently exposed ground, such as drained lakes and emerging shorelines, which we do not observe at Mokka Fiord. There is also less potential for ice segregation and heave in coarse-grained gravel-rich diamict like that observed at Mokka Fiord. The cold climate regime of Axel Heiberg Island, a general lack of evidence of warm-based glaciation, drained lakes, or lacustrine deposits, and permafrost thicknesses of several hundreds of meters measured at Mokka Fiord (Taylor and Judge, 1976; Pollard et al., 1999) suggest permafrost degradation beneath glacial ice followed by permafrost aggradation and segregated ice formation during glacial retreat, as described by Rampton (1988), as well as significant talik formation and subsequent segregated ice formation, to be highly unlikely at Mokka Fiord.

Furthermore, the massive ice exposed by the active thaw slump in Figure 4a exhibits deformation in the ice matrix yet does not reflect any obvious displacement in the overburden as would be expected for segregated ice (e.g., French and Harry, 1990; Coulombe et al., 2019). There is also no evidence of ice dykes as would be expected for injection ice. This massive ice exposure is more characteristic of buried glacial ice, which is more widespread in the High Arctic than previously recognized (Coulombe et al., 2019; O'Neill et al., 2019). Based on the discussion above, it remains unclear how periglacial processes can account for the development of ring forms at Mokka Fiord. Future studies incorporating additional data may help resolve this uncertainty.

5.2 Glacial Origins

Glacial ring forms are common across northern Europe, Scandinavia, and North America (Table 1). Although glacial ring form origins remain debated, their formation is largely attributed to one of the following two main hypotheses: (1) Supraglacial debris concentrations left from the disintegration of stagnant proglacial/ice-marginal ice, including HT type 2 hummocks in Albera, Canada (Evans et al., 2014), Circular Ridges in Norway (Knudsen et al., 2006), Ring Ridge Hummocky moraines in Finland (Aartolahti, 1974), Ice-contact Rings in Saskatchewan, Canada (Parizek, 1969), ring ridge moraines in Nunavut,

Canada (Hibbard et al., 2021), and more (Boulton, 1967; Clayton, 1967; Clayton and Moran, 1974; Eyles, 1979, 1983; Kruger, 1983; Paul, 1983; Clayton et al., 1985; Sollid and Sorbel, 1988; Johnson et al., 1995; Ham and Attig, 1996; Patterson, 1997, 1998; Jennings, 2006; Schomacker, 2008; Evans, 2009); (2) Subglacial diapirism and squeezing of subglacial water-saturated till into basal cavities of disintegrating glacial ice leaving subglacial till ring ridges, including hummocky terrain in Alberta, Canada (Paulen and McClenaghan, 2014), and Pulju moraines in Finland (Sutinen et al., 2014, 2018, 2019; Middleton et al., 2020), and more (Hoppe, 1952; Eyles et al., 1999; Stalker, 1960; Boone and Eyles, 2001; Menzies and Shilts, 2002). Other suggested formation hypotheses include forming from (1) either supraglacial or subglacial processes (Gravenor and Kupsch, 1959; Watson and Watson, 1974; Ross et al., 2019); (2) both supraglacial and subglacial processes (Lagerbäck, 1988); (3) englacial processes (Ebert and Kleman, 2004; Boyes et al., 2021; 2024); (4) ice blocks settling and melting in a drained proglacial or ice-marginal lake leaving predominantly fine-grained till and lacustrine sediments (Dionne, 1978; Mollard, 2000); (5) subglacial meltwater erosion similar to that of drumlins and Rogen moraines, and other transverse moraines (Shaw, 1996; Munro-Stasiuk and Shaw, 1997; Munro-Stasiuk and Sjogren, 2006); and (6) proglacial extrusion of sediment due to over-pressurized groundwater (Bluemle and Clayton, 1984; Bluemle, 1993; Boulton and Caban, 1995; Evans et al., 1999). More details regarding the various types of ring forms and their specific differences are described by Johnson and Clayton (2003) and Hibbard et al. (2021).

There is considerable variation in the scale, landform association, and sedimentology of glacial ring forms (Table 1), yet many are found in present-day farmland and vegetated regions, which likely leads to the preferential preservation of large-scale landforms, and only a handful are composed of coarse-grained sediment (Table 1). Mokka Fiord ring forms are an outlier in that they are both small-scale and occur in course-grained sediments. Additionally, the morphometry, affiliated ice sheet characteristics, and thermal regime (i.e., Innuitian, Laurentide, British-Irish, vs. Fennoscandian Ice Sheets), and/or deposit age of glacial ring forms differ markedly from the Mokka Fiord ring forms (Table 1). Ring forms at Dundas Harbour (Hibbard et al., 2021) are the only glacial ring forms reported in Nunavut and are identical in morphology and morphometry to the ring forms at Mokka Fiord (Table 1; Fig. 8). For example, individual circular closed-cell ring forms at Dundas Harbour (Devon Island) and Mokka Fiord (Axel Heiberg Island) exhibit an identical microtopography consisting of rounded convex ridges, a u-shaped concave central depression with an abrupt change in slope at the ridge-trough transition, miniature grooves where cracks along the ridge apex occur, and gradual outward-facing slopes leading to the mesh (Fig. 8). The sedimentology of ring forms at Dundas Harbour was interpreted as a sandy clast-rich till based on grain size analyses (Hibbard et al., 2021). Although no grain size distribution was done on Mokka Fiord ring forms, field observations indicate the material is composed of sub-rounded clast-rich sand and shows minor evidence of preferred orientation and minimal stratification of sands and gravels in the pits excavated and exposures observed in the field. The sedimentology at Mokka Fiord is most consistent with a glaciofluvial deposit rather than a glacial till.
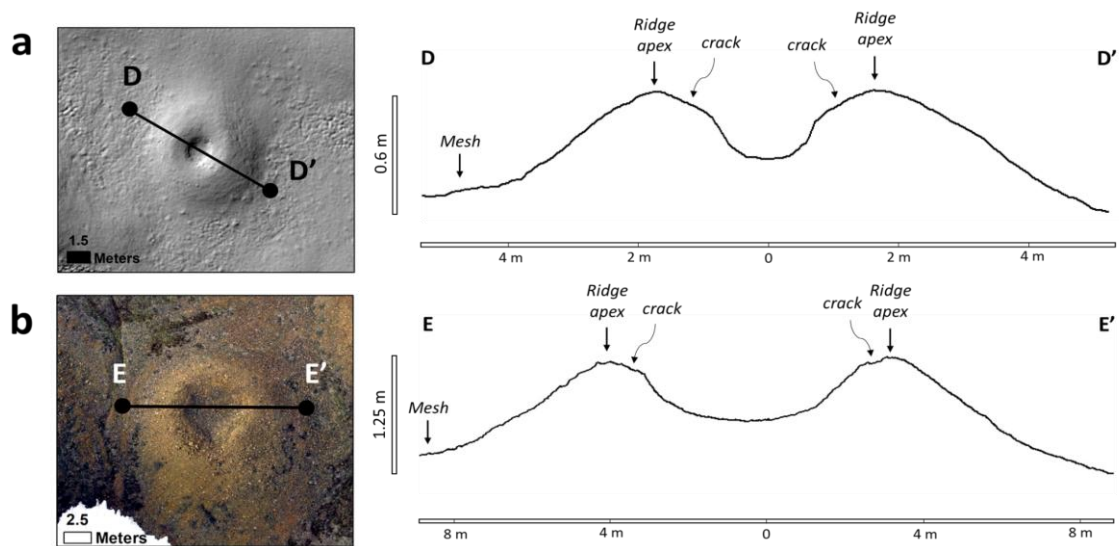
Figure 8: Topographic profiles of circular closed cell ring forms at Mokka Fiord and Dundas Harbour. (a) Example of a circular ring form at Mokka Fiord, Axel Heiberg Island, Nunavut, Canada (D-D'). LiDAR data on the left and topographic profile on the right. The ring form displays rounded convex ridges with cracks running just off the axial trace of the ridge, a u-shaped central trough following an abrupt change of slope from the ridge cracks, and a gently sloping transition into the mesh. (b) Example of a circular ring form at Dundas Harbor on Devon Island, Nunavut, Canada (E-E'). Aerial drone imagery on the left and topographic profile on the right. The ring form displays the same microtopography observed in (a) with a larger diameter. Modified from Hibbard et al. (2021).

Thermal contraction crack polygons are observed at Mokka Fiord and clearly cross-cut the ring forms indicating post-depositional modification of the ring form materials (Figs. 3, 5, S1, Supp. Files). This relationship is also observed at Dundas Harbour (Hibbard et al., 2021). However, polygons at the main Mokka Fiord field site are much more developed and well defined compared to those at Dundas Harbour. For example, the polygon troughs are wider, have raised shoulders with cracks running parallel to the troughs, and have both primary and secondary troughs with well-established ice wedges. This may be the product of longer subaerial exposure at Mokka Fiord as the field site is much farther away from the ice caps compared to the ring forms located at Dundas Harbour (Hibbard et al., 2021). However, roughly 50 km north of Mokka Fiord ice-wedge polygons have been shown to develop pronounced geometries and topography in as little as 50 years (Chartrand et al., 2023), suggesting that modification of the subject ring-forms could be a relatively recent event compared to the proposed Holocene history of the region (discussed in more detail below). In addition to ice-wedge polygons, Mokka Fiord has exposed ice at active thaw slumps, whereas massive ground ice was not immediately observed at Dundas Harbour. Given the proximity to the ice cap and incipient polygon cracks at Dundas Harbour, Mokka Fiord ring forms are likely older than Dundas Harbour ring forms despite being at a higher latitude. Despite their identical morphology and morphometry, the depositional environments were different at Mokka Fjord and Dundas Harbour. Ring forms at Dundas Harbour are interpreted to form from the passive ablation of dead detached ice buried by supraglacial till in a proglacial setting. Ring forms at Mokka Fiord occur within outwash plains in glaciofluvial sediments, motivating two important questions. Do ring forms at Dundas Harbor and

440 Mokka Fiord share similar formation mechanisms or pathways? Or, did they form due to a differing set of circumstances and mechanism, and similarities in present-day morphometry reflects the idea that differing processes can lead to similar outcomes?

Bednarski (1998) describes the Quaternary geomorphology and stratigraphy of northeastern Axel Heiberg Island, which is ~300 km northeast of our field site at Mokka Fiord and lies within the outwash plains emanating from the Princess Margaret

445 Range. The outwash plains described by Bednarski (1998) are reported to host extensive kettled outwash terraces (also referred to as kettled sandar) and kame terraces that consist of ice-contact glaciofluvial coarse gravel associated with kettles and kames that range from 30−50 m in relief, ice-contact ridges, and active slumping, all features that indicate the presence of buried glacial ice (Dredge et al., 1999). Kame terraces are ice-marginal/ice-contact features that form alongside meltwater channels and are in contact with glacial ice. They can be easily confused with fluvial or outwash terraces (i.e., sandar) (Menzies, 2002).

450 However, kame terraces typically have multiple steps/terraces on one side of a channel that have varying gradients and elevations to terraces on the opposite side of the channel (e.g., Gray, 1975; Sissons, 1982), much like what we observe at Mokka Fiord. Kame terraces are mostly composed of glaciofluvial sands and gravels from lateral meltwater channels; however, supraglacial and englacial till can accumulate on top of glaciofluvial sediments (e.g., Levson and Rutter, 1989). Kame terraces are often associated with kettle and kame topography, hummocky moraines, buried glacial ice, and eskers (Mckenzie, 1969;

455 McKenzie and Goodwin, 1987; Benn and Evans, 2010), much like what we observed at Mokka Fiord (e.g., Figs. 3d and 4a).

We hypothesize that the ring forms observed at Mokka Fiord are inherently linked to a glacial origin and history. Our hypothesis is supported by both regional and local observations of depositional conditions, terrain features, associated landforms, ground ice conditions, and exposed massive ice structures, in addition to the cold climate and glacial thermal regime

460 of the region. We speculate that Mokka Fiord ring forms are part of a kame terrace similar to those described by Bednarski (1998), further suggesting ice-marginal deposition of coarse-grained glaciofluvial sediment and supraglacial till over detached glacial ice, rather than strictly from a morainic origin as suggested for ring forms at Dundas Harbour (Hibbard et al., 2021). Based on our interpretation, we examine the environmental conditions, ice sheet thermal regime, and the timing of deposition, preservation, and degradation required to produce Mokka Fiord ring forms (Fig. 9 and 10). Based on a glacial origin hypothesis,

465 we propose a plausible sequence of events in the vicinity of Mokka Fiord that aligns with existing geologic data. Marine-based ice largely disappeared by 9 ka BP, leaving mostly land-based ice on Axel Heiberg and other islands (England et al., 2006). At this time, our field site at Mokka Fiord would have been covered by ice, likely within a polythermal environment throughout the Holocene (Fig. 9 - Stage 1). As land-based ice thinned and retreated (Fig. 9 - Glacial Stage 2), ice would have preferentially occupied topographic lows, while supraglacial till and glaciofluvial runoff deposited sediment, burying ice margins and

470 facilitating their detachment from the main ice body. Continued retreat left detached glacial ice buried in outwash plains and ice-marginal terraces, such as detached snout or marginal ice (Fig. 9 - Glacial Stage 3). Over time, the remnant buried glacial ice degraded, forming ring forms through topographic inversion (Fig. 10), while periglacial processes progressively overprinted and modified the landscape, continuing to the present day (Fig. 9 - Glacial Stage 4). Partial or complete melt out

of buried glacial ice may have occurred across the Mokka Fiord area (Fig. 10). The thick permafrost and cold polar desert
475 climate on Axel Heiberg Island likely promote a "stable surface stage," where partial melt out proceeds until thawed materials
insulate the underlying ice, allowing permafrost to preserve the relict ice. Therefore, ring forms may continue to form in the
present-day as buried ice ablates.

Glacial Hypothesis

STAGE 1: Land-based ice (~9 ka BP)

STAGE 2: Glacial retreat & ice localization (~8.5 ka BP)

STAGE 3: Continued ice retreat, ice detachment & burial (~8 ka BP)

STAGE 4: Ice degradation & formation of ring forms (Present Day)
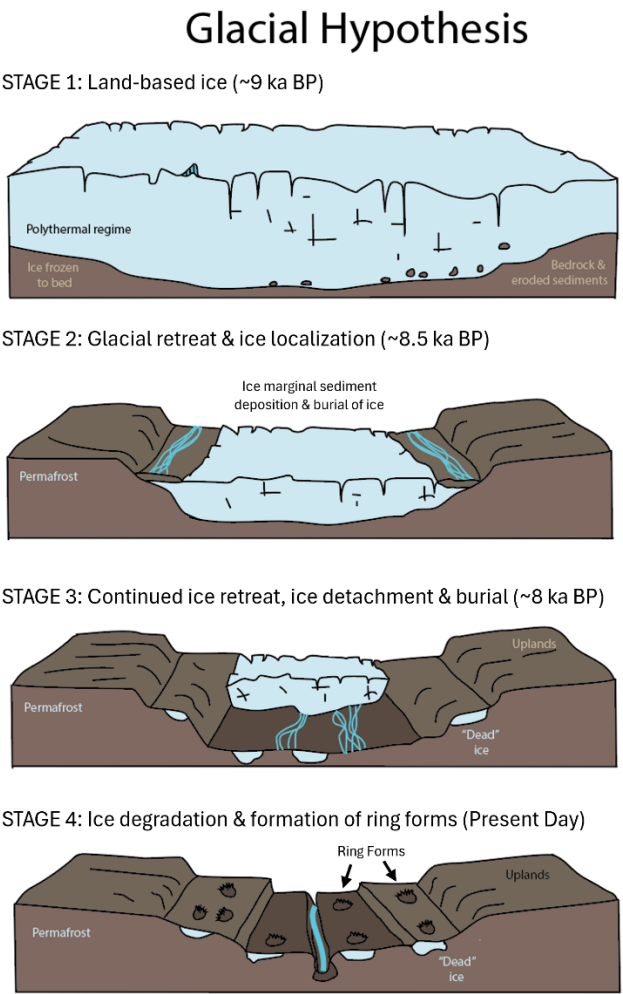
Figure 9: A simplified landscape evolution model for the formation of Mokka Fiord ring forms. Stage 1 illustrates the study area
480 **covered by land-based ice around 9 ka BP (based on England et al, 2006) within a polythermal glacial environment. Stage 2 depicts**
the thinning and retreat of land-based ice, with ice occupying topographic lows. During this stage, supraglacial till and glaciofluvial
runoff deposit sediments, burying ice margins and promoting their detachment from the main ice body. Stage 3 shows continued
retreat with glacial ice becoming detached and buried in the outwash plains and kame terrace remnants. Stage 4 features a mature
meltwater channel system with remnant buried glacial ice. The ongoing degradation of buried ice leads to the formation of ring
485 **forms (starting prior to Stage 4), while periglacial processes further modify the landscape. Modified from Flint (1971).**
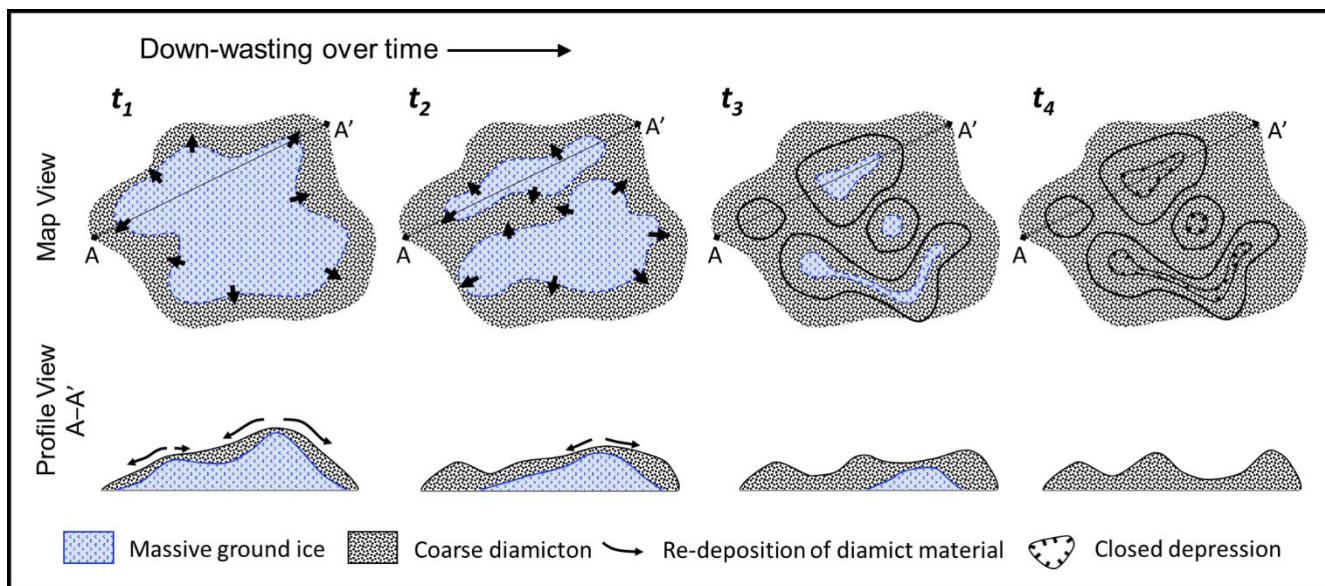
Figure 10: A simplified model for the formation of ring forms modified from Knudsen et al. (2006) and Hibbard et al. (2021). Over time (t) detached glacial ice under a layer of coarse-grained diamicton will begin to down waste and separate into individual ice blocks (t1–t3). Diamict is transferred from topographic highs to topographic lows as ice ablates (t1–t2). Ridges and troughs begin to form where diamict accumulates (t2–t3). If ice fully ablates, a complex series of ridges and troughs at their maximum relief is left (t4). Periglacial modification can begin at any time after ridges form. Ring forms at Mokka Fiord may be at any stage.

6 Summary and Conclusions

Ring forms near Mokka Fiord on Axel Heiberg Island in Nunavut, Canada exhibit a circular, elongated, sinuous, and/or anastomosing morphology as a series of ridges and troughs. They occur on multiple terraces and within the floodplain of a glacial meltwater channel (Fig. 2). Thaw slumps (Fig. 4), active lobate slumping (Fig. 7), and thermokarst degradation (Fig. 3e) found among the ring forms suggest the presence of massive ice. Ice wedge polygons cross-cut ring forms (Figs. 3 and 6) suggesting periglacal modification of the landscape following the formation of the ring forms.

We used regional and local observations coupled with comparisons to other morphologically similar periglacial and glacial features (Table 1) to elucidate an origin. Although many periglacial features share a remarkable resemblance to Mokka Fiord ring forms, many lines of evidence point towards a glacial origin. Axel Heiberg Island has minimal evidence of wet-based glaciation and is thought to have maintained a cold climate regime hosting polythermal to bold based glaciers throughout the Holocene. The cold glacial regime likely provided limited water supply to continuously feed taliks for lithalsa or other ice segregation features. Permafrost is hundreds of meters thick at the Mokka Fiord site and was unlikely to be completely obliterated when glaciers covered the region. Massive ice exposed at the Mokka Fiord site displays deformation in the ice matrix and no effect to the overburden suggesting deformed glacial ice was detached and buried. Multiple terraces containing

ring forms in addition to observations of kame terraces and kettled outwash ~300 km north of our field site. Additionally,
potential kames were observed amidst ring forms. Our observations suggest a glacial origin for Mokka Fiord ring forms. We
510   interpret Mokka Fiord ring forms to be an ice-marginal features forming from the deposition of glaciofluvial sediments over
detached buried glacial ice resulting in kame terraces. Uneven degradation of the buried glacial ice leads to the topographic
inversion of overlying sediment forming the Mokka Fiord ring form's hummocky expression. This formation mechanism
supports a predominantly polythermal glacial environment with limited water supply throughout much of the Holocene.

515   Limited examples of coarse-grained glacial ring forms, let alone small-scale, have been documented in the literature. Glacial
ring forms at Dundas Harbour on Devon Island are the only other glacial ring forms documented in Nunavut and bear
remarkable resemblance to the ring forms at Mokka Fiord. The small-scale nature of these high arctic features is likely due to
their relatively recent formation, lack of vegetation and human activity, and dry desert climate preserving these pristine
examples of glacial ring forms.

520   **Competing Interests**

The contact author has declared that none of the authors have any competing interests.

Acknowledgements

We would like to thank the Inuit of the Qikiqtani Region (one of the three regions in the territory of Nunavut). Fieldwork was
carried out on their land in Nunavut. We would like to thank the community of Qausuittuq (Resolute Bay) for welcoming us
525   during our stay in the summer of 2019. Logistical support from the Polar Continental Shelf Program (NRCan) is gratefully
acknowledged. Funding was provided by a Canadian Space Agency (CSA) Flights and Fieldwork for the Advancement of
Science and Technology (FAST) grant and Natural Sciences and Engineering Research Council of Canada (NSERC)
Discovery Grant Northern Supplement to GRO. SH was supported by an appointment to the NASA Postdoctoral Program at
the Jet Propulsion Laboratory, California Institute of Technology, administered by Oak Ridge Associated Universities under
530   a contract with NASA (80HQTR21CA005). The research was carried out at the Jet Propulsion Laboratory, California Institute
of Technology, under a contract with the National Aeronautics and Space Administration (80NM0018D0004). Reference
herein to any specific commercial product, process, or service by trade name, trademark, manufacturer, or otherwise, does not
constitute or imply its endorsement by the United States Government or the Jet Propulsion Laboratory, California Institute of
Technology. The authors would like to thank Academy of Finland (Coe-LaSR, MS-PLS 300066) and Strategic Research
535   Council at the Academy of Finland project "Competence Based Growth Through Integrated Disruptive Technologies of 3D
Digitalization, Robotics, Geospatial Information and Image Processing/Computing - Point Cloud Ecosystem
(293389/314312)." Geospatial support for this work provided by the Polar Geospatial Center under NSF-OPP awards 1043681

and 1559691 allowed for the use of ArcticDEM data for this project. Figures throughout this article were created using ArcGIS® software by Esri. ArcGIS® and ArcMap™ are the intellectual property of Esri and are used herein under license.

540 Copyright © Esri. All rights reserved. For more information about Esri® software, please visit www.esri.com. We would also like to thank Inuit Tapiriit Kanatami for their map of Inuit Nunangat, which was used for referencing Inuktut geographical terms.

References

Aartolahti, T.: Ring ridge hummocky moraines in northern Finland, Fenn. - Int. J. Geogr. 134, 1974.

545

Allen, C.R., O'Brien, R.M.G. and Sheppard, S.M.F.: The chemical and isotopic characteristics of some northeast Greenland surface and pingo waters. *Arctic and Alpine Research*, *8*(3), pp.297-317, 1976.

Andersen, D.T., Pollard, W.H., McKay, C.P., Heldmann, J.: Cold springs in permafrost on Earth and Mars, J. Geophys. Res.

550 E Planets 107, 4–1. https://doi.org/10.1029/2000je001436, 2002.

Arp, C. D., Jones, B. M., Urban, F. E. and Grosse, G.: Hydrogeomorphic processes of thermokarst lakes with grounded-ice and floating- ice regimes on the Arctic coastal plain, Alaska, Hydrol. Processes, 25, 15, 2422–2438, doi:10.1002/hyp.8019, 2011.

555

Balkwill, H.R.: Evolution of Sverdrup Basin, Arctic Canada, AAPG Bull. (American Assoc. Pet. Geol. 62, 1004–1028. https://doi.org/10.1306/c1ea4f86-16c9-11d7-8645000102c1865d, 1978.

Bednarski, J.M.: Quaternary history of Axel Heiberg Island bordering Nansen Sound, Northwest Territories, emphasizing the

560 last glacial maximum, Can. J. Earth Sci. 35, 520–533. https://doi.org/10.1139/e97-124, 1998.

Blatter, H.: On the thermal regime of an Arctic valley glacier: a study of White Glacier, Axel Heiberg Island, NWT, Canada, Journal of Glaciology, 33, 114, 200–211. https://doi.org/10.3189/S0022143000008704, 1987.

565 Boone, S.J., Eyles, N.: Geotechnical model for great plains hummocky moraine formed by till deformation below stagnant ice. Geomorphology 38 (1), 109–124. https://doi.org/10.1016/S0169-555X(00)00072-6, 2001.

Boulton, G.S.: Modern Arctic glaciers as depositional models for former ice sheets. J. Geol. Soc. Lond. 128 (4), 361–393. https://doi.org/10.1144/gsjgs.128.4.0361, 1972.

570

Boyes, B.M., Pearce, D.M. and Linch, L.D.: Glacial geomorphology of the Kola Peninsula and Russian Lapland. Journal of Maps, 17, 2, 497–515, https://doi.org/10.1080/17445647.2021.1970036, 2021.

Boyes, B.M., Pearce, D.M., Linch, L.D. and Nash, D.J.: Younger Dryas and Early Holocene ice-margin dynamics in northwest
575   Russia. Boreas, https://doi.org/10.1111/bor.12653, 2024.

Burn, C.R., Tundra lakes and permafrost, Richards Island, western Arctic coast, Canada. Canadian Journal of Earth Sciences, https://doi.org/10.1139/e02-035, 2002.

580   Calmels, F., Allard, M. and Delisle, G.: Development and decay of a lithalsa in Northern Quebec: a geomorphological history, Geomorphology, 97(3-4), p. 287-299. https://doi.org/10.1016/j.geomorph.2007.08.013, 2008.

Chartrand, S.M., Jellinek, A.M., Kukko, A. Grau Galofre, A., Osinski, G.R., Hibbard, S.: High Arctic channel incision modulated by climate change and the emergence of polygonal ground. Nat Commun 14, 5297. https://doi.org/10.1038/s41467-023-40795-9, 2023.
585

Clayton, L.: Karst Topography on Stagnant Glaciers, Journal of Glaciology, 5, 37, 107–112. https://doi.org/10.3189/S0022143000028628, 1964.

590   Clayton, L.: Stagnant glacier features of the Missouri Coteau in North Dakota. North Dakota Geological Survey Miscellaneous Series. 30, pp. 25–46, 1967.

Clayton, L., Moran, S.R.: A glacial process-form model. In: Coates, D.R. (Ed.), Glacial Geomorphology. SUNY-Binghamton Publications in Geomorphology, Binghamton, NY, pp. 89–119, 1974.
595

Coulombe, S., Fortier, D., Lacelle, D., Kanevskiy, M. and Shur, Y.: Origin, burial and preservation of late Pleistocene-age glacier ice in Arctic permafrost (Bylot Island, NU, Canada). *The Cryosphere*, *13*(1), pp.97-111, 2019.

Constable, A.J., Harper, S., Dawson, J., Mustonen, T., Piepenburg, D., Rost, B., Bokhorst, S., Boike, J., Cunsolo, A., Derksen,
600   C. and Feodoroff, P.: Climate change 2022: Impacts, adaptation and vulnerability: Cross-chapter paper 6: Polar regions, 2022.

Demidov, V., Demidov, N., Verkulich, S. and Wetterich, S.: Distribution of pingos on Svalbard. *Geomorphology*, *412*, p.108326, 2022.

605   Dredge, L.A., Kerr, D.E. and Wolfe, S.A.: Surface materials and related ground ice conditions, Slave Province, NWT, Canada. Canadian Journal of Earth Sciences , 36, 7, pp.1227-123, https://doi.org/10.1139/e98-087. 1999.

Dyke, A.S., Dredge, L.A., Hodgson, D.A.: North America deglacial marine- and lake-limit surfaces, in: Geographie Physique et Quaternaire. Presses de l'Universite de Montreal, pp. 155–185. https://doi.org/10.7202/014753ar, 2005.

610

Dyke, A.S. and Evans, D.J.: Ice-marginal terrestrial landsystems: northern Laurentide and Innuitian ice sheet margins. In: Glacial landsystems, Arnold, London, 143–165, 2003.

Ebert, K., Kleman, J.: Circular moraine features on the Varanger Peninsula, northern Norway, and their possible relation to
615   polythermal ice sheet coverage. Geomorphology 62, 159–168. https://doi.org/10.1016/j.geomorph.2004.02.009, 2004.

Embleton, C., King, C. A. M.: Glacial geomorphology. Edward Arnold Publishers Ltd. London, UK, 1975.

Embry, A., Beauchamp, B.: Chapter 13 Sverdrup Basin, in: Sedimentary Basins of the World. Elsevier, pp. 451–471.
620   https://doi.org/10.1016/S1874-5997(08)00013-0, 2008.

England, J., Atkinson, N., Bednarski, J., Dyke, A.S., Hodgson, D.A., Ó Cofaigh, C.: The Innuitian Ice Sheet: configuration, dynamics and chronology. Quat. Sci. Rev. 25, 689–703. https://doi.org/10.1016/j.quascirev.2005.08.007, 2006.

625   Environment Canada: Canadian Climate Normals 1981–2010 Station Data. Eureka A station, Nunavut. Government of Canada. http://climate.weather.gc.ca/climate_normals/ (accessed 12 June 2021), 2021.

Esri: "Imagery" [basemap]. Scale Not Given. "World Imagery". July 18, 2018. https://www.arcgis.com/home/item.html?id=10df2279f9684e4a9f6a7f08febac2a9. (accessed 20 June 2020), 2018.
630

Evans, D.J.A.: Controlled moraines: origins, characteristics and palaeoglaciological implications. Quat. Sci. Rev. 28 (3), 183–208. https://doi.org/10.1016/j.quascirev.2008.10.024, 2009.

Evans, D.J., Young, N.J. and Cofaigh, C.Ó.: Glacial geomorphology of terrestrial-terminating fast flow lobes/ice stream
635   margins in the southwest Laurentide Ice Sheet. Geomorphology, 204, 86–113, https://doi.org/10.1016/j.geomorph.2013.07.031, 2014.

Eyles, N.: Facies of supraglacial sedimentation on Icelandic and alpine temperate glaciers. Can. J. Earth Sci. 16, 1341–1361, 1979.

640

Eyles, N.:Modern Icelandic glaciers as depositionalmodels for 'hummocky moraine' in the Scottish Highlands. In: Evenson, E.B., Schluchter, C., Rabassa, J. (Eds.), Tills and Related Deposits. Balkema, Rotterdam, pp. 47–59, 1983.

Eyles, N., Boyce, J.I., Barendregt, R.W.: Hummocky moraine: sedimentary record of stagnant Laurentide Ice Sheet lobes

645   resting on soft beds. Sediment. Geol. 123 (3), 163–174. https://doi.org/10.1016/S0037-0738(98)00129-8, 1999.

Fairbridge, R.W.: Inversion (of topography, relief). In: Geomorphology. Encyclopedia of Earth Science. Springer, Berlin, Heidelberg. https://doi.org/10.1007/3-540-31060-6_193, 1968.

650   Flint, R.F.: Glacial and Quaternary Geology. Wiley, 1971.

French, H.M.: Ice cored mounds and patterned ground, Southern Banks Island, Western Canadian Arctic. Geografiska Annaler Series A, Physical Geography, 53, 32–38. https://doi.org /10.1080/04353676.1971.11879832, 1971.

655   French, H.M. and Harry, D.G.: Observations on buried glacier ice and massive segregated ice, western Arctic coast, Canada. Permafrost and Periglacial Processes, 1, 1, 31-43. https://doi.org/10.1002/ppp.3430010105, 1990.

Geological Survey of Canada: Surficial geology, western Fosheim Peninsula and eastern Axel Heiberg Island, Nunavut, NTS 49-G and 340-B southwest; Geological Survey of Canada, Canadian Geoscience Map 392 (Surficial Data Model v.2.3.14

660   conversion of Open File 501), scale 1:125 000. https://doi.org/10.4095/313535, 2022.

Gravenor, C.P., Kupsch, W.O.: Ice-Disintegration Features in Western Canada. J. Geol. 67, 48–64. https://doi.org/10.1086/626557, 1959.

665   Haines-Young, R.H., Petch., R.J.: Multiple working hypotheses: equifinality and the study of landforms. Trans. Inst. Br. Geogr. 8 (4), 458–466. https://doi.org/10.2307/621962, 1983.

Hallet, B.: Stone circles: Form and soil kinematics. Philosophical Transactions of the Royal Society of London. Series A: Mathematical, Physical, and Engineering Sciences, 371, 2004, 20120357–20120357. https://doi.org/10.1098/rsta.2012.0357,

670   2013.

Hallet, B., Prestrud, S.: Dynamics of periglacial sorted circles in western Spitsbergen. Quat. Res. 26 (1), 81–99. https://doi.org/10.1016/0033-5894(86)90085-2, 1986.

675   Ham, N.R., Attig, J.W.: Ice wastage and landscape evolution along the southern margin of the Laurentide Ice Sheet, north-central Wisconsin. Boreas 25 (3), 171–186, https://doi.org/10.1111/j.1502-3885.1996.tb00846.x, 1996.

Harrison, J.C., Jackson, M.P.A.: Exposed evaporite diapirs and minibasins above a canopy in central Sverdrup Basin, Axel Heiberg Island, Arctic Canada. Basin Res. 26, 567–596. https://doi.org/10.1111/bre.12037, 2014.

680

Henkemans, E.: Geochemical characterization of groundwaters, surface waters and water-rock interaction in an area of continuous permafrost adjacent to the Greenland ice sheet, Kangerlussuaq, southwest Greenland, 2016.

Hibbard, S. M., Osinski, G. R., Godin, E.: Vermicular Ridge Features on Dundas Harbour, Devon Island, Nunavut.
685   Geomorphology, 395. https://doi.org/10.1016/j.geomorph.2021.107947, 2021.

Holmes, G.W., Hopkins, D.M. and Foster, H.L.: Pingos in central Alaska (p. H1-H40). Washington, DC: US Government Printing Office, 1968.

690   Hoppe, G.: Hummocky Moraine Regions with special reference to the interior of Norrbotten. Geogr. Ann. 34, 1–72. https://doi.org/10.2307/520144, 1952.

Hyyppä, E., Kukko, A., Kaijaluoto, R., White, J.C., Wulder, M.A., Pyörälä, J., Liang, X., Yu, X., Wang, Y., Kaartinen, H., Virtanen, J.P., Hyyppä, J.: Accurate derivation of stem curve and volume using backpack mobile laser scanning. ISPRS J.
695   Photogramm. Remote Sens. 161, 246–262. https://doi.org/10.1016/j.isprsjprs.2020.01.018, 2020.

Jennings, C.E.: Terrestrial ice streams—a viewfromthe lobe. Geomorphology 75 (1), 100–124. https://doi.org/10.1016/j.geomorph.2005.05.016, 2006.

700   Johnson, M.D., Clayton, L.: Chapter 10: Supraglacial landsystems in lowland terrain. In: Evans, D.J.A. (Ed.), Glacial Landsystems. London, 228–258, 2003.

Johnson, M.D., Mickelson, D.M., Clayton, L., Attig, J.W.,: Composition and genesis of glacial hummocks, western Wisconsin, USA. Boreas 24 (2), 97–116. https://doi.org/10.1111/j.1502-3885.1995.tb00630.x, 1995.

705

Jorgenson, M. T., and Y. Shur: Evolution of lakes and basins in northern Alaska and discussion of the thaw lake cycle, J. Geophys. Res., 112, F02S17, https://doi.org/10.1029/2006JF000531, 2007.

Kääb, A., Girod, L., Berthling, I.: Surface kinematics of periglacial sorted circles using structure-from-motion technology. Cryosphere 8 (3), 1041–1056. https://doi.org/10.5194/tc-8-1041-2014, 2014.

Kessler, M.A., Murray, A.B., Werner, B.T., Hallet, B.: A model for sorted circles as self organized patterns. J. Geophys. Res. Solid Earth 106 (B7), 13287–13306. https://doi.org/10.1029/2001JB000279, 2001.

Knudsen, C.G., Larsen, E., Sejrup, H.P., Stalsberg, K.: Hummocky moraine landscape on Jæren, SW Norway-implications for glacier dynamics during the last deglaciation. Geomorphology 77, 153–168. https://doi.org/10.1016/j.geomorph.2005.12.011, 2006.

Krüger, J., Kjær, K.H. and Schomacker, A.: 7 Dead-Ice Environments: A Landsystems Model for a Debris-Charged, Stagnant Lowland Glacier Margin, Kötlujökull. Developments in Quaternary Sciences, 13, 105–126. https://doi.org/10.1016/S1571-0866(09)01307-4, 2010.

Kukko, A., Kaartinen, H., Hyyppä, J., Chen, Y.: Multiplatform mobile laser scanning: Usability and performance. Sensors (Switzerland). https://doi.org/10.3390/s120911712, 2012.

Kukko, A., Kaijaluoto, R., Kaartinen, H., Lehtola, V. V., Jaakkola, A., Hyyppä, J.: Graph SLAM correction for single scanner MLS forest data under boreal forest canopy. ISPRS J. Photogramm. Remote Sens. 132, 199–209. https://doi.org/10.1016/j.isprsjprs.2017.09.006, 2017.

Kukko, A., Kaartinen, H., Osinski, G. and Hyyppä, J.: Modeling Permafrost Terrain Using Kinematic, Dual-Wavelength Laser Scanning. ISPRS Annals of the Photogrammetry, Remote Sensing and Spatial Information Sciences, 2, 749–756. https://doi.org/10.5194/isprs-annals-V-2-2020-749-2020, 2020.

Lagerbäck, R.: The Veiki moraines in northern Sweden-widespread evidence of an Early Weichselian deglaciation. Boreas, 17, 4, 469–486. https://doi.org/10.1111/j.1502-3885.1988.tb00562.x, 1988.

Liestøl, O.: Pingos, springs, and permafrost in Spitsbergen. Norsk Polarinstitutt Årbok. p. 7-29, 1977.

Liang, X., Wang, Y., Jaakkola, A., Kukko, A., Kaartinen, H., Hyyppä, J., Honkavaara, E., Liu, J.: Forest data collection using

740 terrestrial image-based point clouds from a handheld camera compared to terrestrial and personal laser scanning. IEEE Trans. Geosci. Remote Sens. 53, 5117–5132, 2015.

Lindsay, J.B.: The Whitebox Geospatial Analysis Tools project and open-access GIS. Proceedings of the GIS Research UK 22nd Annual Conference, The University of Glasgow, 16-18 April, https://doi.org/10.13140/RG.2.1.1010.8962, 2014.

745

Lindsay, J.B.: Whitebox GAT: A case study in geomorphometric analysis. Computers and Geosciences, 95: 75–84. https://doi.org/10.1016/j.cageo.2016.07.003, 2016.

Lundqvist, J.: Rogen (ribbed) moraine—identification and possible origin. Sedimentary Geology, 62, 2–4, 281–292.

750 https://doi.org/10.1016/0037-0738(89)90119-X, 1989.

Mackay, J.R.: The Mackenzie Delta area, N.W. T.; Geographical Branch, Memoir 8, 1963.

Mackay, J.R: The Mackenzie Delta area, Northwest Territories. Geological Survey of Canada Report 23, Energy, Mines and

755 Resources Canada https://doi.org/10.4095/119932., 1974.

Mackay, J.R.: Pingo Growth and collapse, Tuktoyaktuk Peninsula Area,Western Arctic Coast, Canada: a long-term field study. Géog. Phys. Quatern. 52 (3), 271–323. https://doi.org/10.7202/004847ar, 1998.

760 Mackay, J. R., Burn, C. R.: The first 20 years (1978–1979 to 1998–1999) of active layer development, Illisarvik experimental drained lake site, western Arctic coast, Canada. Canadian Journal of Earth Sciences, 39, 1657–1674, 2002.

Mackay, J.R. and Dallimore, S.R.: Massive ice of the Tuktoyaktuk area, western Arctic coast, Canada. Canadian Journal of Earth Sciences, 29, 6, 1235-1249. https://doi.org/10.1139/e92-099, 1992.

765

Mckenzie, G.D.: Observations on a Collapsing Kame Terrace In Glacier Bay National Monument, South-Eastern Alaska. J. Glaciol. 8, 413–425. https://doi.org/10.3189/s0022143000027003, 1969.

McKenzie, G.D., Goodwin, R.G.: Development of Collapsed Glacial Topography in the Adams Inlet Area, Alaska, U.S.A. J.

770 Glaciol. 33, 55–59. https://doi.org/10.3189/s0022143000005347, 1987.

Menzies, J., Shilts, W.W.: Subglacial environments. In: Menzies, J. (Ed.), Modern & Past Glacial Environments. Butterworth-Heinemann, pp. 183–278, 2002.

775 Middleton, M., Heikkonen, J., Nevalainen, P., Hyvönen, E. and Sutinen, R.: Machine learning-based mapping of micro-topographic earthquake-induced paleo-Pulju moraines and liquefaction spreads from a digital elevation model acquired through laser scanning. Geomorphology, 358, 107099. https://doi.org/10.1016/j.geomorph.2020.107099, 2020.

Moore, P. L.: Numerical Simulation of Supraglacial Debris Mobility: Implications for Ablation and Landform Genesis. Front.
780 Earth Sci. 9:710131. https://doi.org/10.3389/feart.2021.710131, 2021.

Morse, P.D., and Burn, C.R.: Perennial frost blisters of the outer Mackenzie Delta, western Arctic coast, Canada. Earth Surface Processes and Landforms, 39: 200–213. https://doi.org/10.1002/esp.3439, 2014.

785 Müller, F.: Analysis of some stratigraphic observations and radiocarbon dates from two pingos in the Mackenzie Delta area, NWT. Arctic, 15(4), p.279-288, 1962.

Ó Cofaigh, C., England, J., Zreda, M.: Late Wisconsinan glaciation of southern Eureka Sound: Evidence for extensive Innuitian ice in the Canadian High Arctic during the Last Glacial Maximum. Quat. Sci. Rev. 19, 1319–1341.
790 https://doi.org/10.1016/S0277-3791(99)00104-3, 2000.

Ó Cofaigh, C., Evans, D., and England, J.: Ice marginal terrestrial landsystems: Sub-polar glacier margins of the Canadian and Greenland high arctic. In Glacial Landsystems, ed. D. Evans, Chapter 3, 2003.

795 Ó Cofaigh, C., Lemman, D.S., Evans, D.J.A. and Bednarski, J.: Glacial landform-sediment assemblages in the Canadian High Arctic and their implications for late Quaternary glaciations. Annals of Glaciology, 28, 195–201. https://doi.org/10.3189/172756499781821760, 1999.

Ommanney, C.S.: A study in glacier inventory: the ice masses of Axel Heiberg Island, Canadian Arctic Archipelago, 1969.
800
O'Neill, H.B., Wolfe, S.A. and Duchesne, C.: New ground ice maps for Canada using a paleogeographic modelling approach. The Cryosphere, 13(3), p.753-773. https://doi.org/10.5194/tc-13-753-2019, 2019.

Parizek, R.R.: Glacial ice-contact rings and ridges. United States Contributions to Quaternary Research. Geological Society of
805 America Special Paper 123, pp. 49–102, 1969.

Patterson, C. J.: Southern Laurentide ice lobes were created by ice streams: Des Moines Lobe in Minnesota, USA. Sediment. Geol., 111, 1, 249–261. https://doi.org/10.1016/S0037-0738(97)00018-3, 1997.

810 Patterson, C.J.: Laurentide glacial landscapes: the role of ice streams. Geology 26 (7), 643–646. https://doi.org/10.1130/0091-7613(1998)026<0643:LGLTRO>2.3.CO;2, 1998.

Paul, M.A.: The supraglacial landsystem. In: Eyles, N. (Ed.), Glacial Geology, Oxford, pp. 71–90 https://doi.org/10.1016/B978-0-08-030263-8.50009-9, 1983.

815

Paulen, R.C., McClenaghan,M.B.: Late wisconsin ice-flow history in the buffalo head hills kimberlite field, north-central alberta. Can. J. Earth Sci. 52 (1), 51–67. https://doi.org/10.1139/cjes-2014-0109, 2014.

Pissart, A.: Palsas, lithalsas and remnants of these periglacial mounds. A progress report. Progress in Physical Geography: 820 Earth and Environment, 26: 605–621. https://doi.org/10.1191/0309133302pp354ra, 2002.

Pissart, A., French, H.M.: Pingo investigations, north-central Banks Island, Canadian Arctic. Can. J. Earth Sci. 13 (7), 937–946. https://doi.org/10.1139/e76-096, 1976.

825 Pissart, A., French, H.M.: The origin of pingos in regions of thick permafrost, western Canadian Arctic. Quaestiones Geographicae 4, 149–160. http://hdl.handle.net/2268/248067, 1977.

Pollard, W. and Bell, T.: Massive ice formation in the Eureka Sound Lowlands: A landscape model. In Proceedings, Seventh International Permafrost Conference (pp. 903-908). Laval, Quebec City, Quebec, Canada: Université Laval, Centre d'etudes 830 nordiques, Collection Nordicana, 1998.

Pollard, W., Omelon, C., Andersen, D., McKay, C.: Perennial spring occurrence in the Expedition Fiord area of western Axel Heiberg Island, Canadian High Arctic. Can. J. Earth Sci. 36, 105–120. https://doi.org/10.1139/e98-097, 1999.

835 Porter, C., Morin, P., Howat, I., Noh,M., Bates, B., Peterman, K., Keesey, S., Schlenk, M., Gardiner, J., Tomko, K.,Willis, M., Kelleher, C., Cloutier, M., Husby, E., Foga, S., Nakamura, H., Platson, M., Wethington, M. J., Williamson, C., Bauer, G., Enos, J., Arnold, G., Kramer, W., Becker, P., Doshi, A., D'Souza, C., Cummens, P., Laurier, F., Bojesen, M.: ArcticDEM. https://doi.org/10.7910/DVN/OHHUKH, (Harvard Dataverse, V1), (accessed 23 May 2022), 2018.

840   Rampton, V. N.: Quaternary Geology of the Tuktoyaktuk Coastlands, Northwest Territories, Memoir 423, Geological Survey of Canada, Ottawa, ON, Canada, 1988.

Ross, N., Brabham, P., Harris, C.: The glacial origins of relict "pingos", Wales, UK. Ann. Glaciol. 60, 138–150. https://doi.org/10.1017/aog.2019.40, 2019.

845

Russell, A.J., Roberts, M.J., Fay, H., Marren, P.M., Cassidy, N.J., Tweed, F.S., Harris, T.: Icelandic jökulhlaup impacts: Implications for ice-sheet hydrology, sediment transfer and geomorphology. Geomorphology 75, 33–64. https://doi.org/10.1016/j.geomorph.2005.05.018, 2006.

850   Schmertmann, J.H., Taylor, R.S.: Quantitative data from a patterned ground site over permafrost. U.S. Army Cold Regions Research and Engineering Laboratory Research Report. 96, p. 76, 1965.

Schomacker, A.: What controls dead-ice melting under different climate conditions? A discussion. Earth-Sci. Rev. 90 (3), 103–113. https://doi.org/10.1016/j.earscirev.2008.08.003, 2008.

855

Sutinen, R., Hyvönen, E., Middleton, M., Ruskeeniemi, T.: Airborne LiDAR detection of postglacial faults and Pulju moraine in Palojärvi, Finnish Lapland. Glob. Planet. Chang. 115, 24–32. https://doi.org/10.1016/j.gloplacha.2014.01.007, 2014.

Sutinen, R., Hyvönen, E., Middleton, M., Airo, M.L.: Earthquake-induced deformations on ice-stream landforms in Kuusamo, 860   eastern Finnish Lapland. Glob. Planet. Chang. 160, 46–60. https://doi.org/10.1016/j.gloplacha.2017.11.011, 2018.

Sutinen, R., Hyvönen, E., Liwata-Kenttälä, P., Middleton, M., Ojala, A., Ruskeeniemi, T., Sutinen, A., Mattila, J.: Electrical-sedimentary anisotropy of landforms adjacent to postglacial faults in Lapland. Geomorphology 326, 213–224. https://doi.org/10.1016/j.geomorph.2018.01.008, 2019.

865

Taylor, A.E., Judge, A.S.: Canadian Geothermal Data Collection: Northern Wells. Ottawam, 1976.

Thompson S, Benn DI, Mertes J, Luckman A.: Stagnation and mass loss on a Himalayan debris-covered glacier: Processes, patterns and rates. Journal of Glaciology 62, 233, 467–485. https://doi.org/10.1017/jog.2016.37, 2016.

870

Thomson, L.I., Osinski, G.R., Ommanney, C.S.L.: Glacier change on Axel Heiberg Island, Nunavut, Canada. J. Glaciol. 57, 1079–1086. https://doi.org/10.3189/002214311798843287, 2011.

Thorsteinsson, R.: Geology, Eureka Sound North, District of Franklin. Geological Survey of Canada, "A" Series Map 1302A,
875   1 sheet, https://doi.org/10.4095/109125, 1971a.

Thorsteinsson, R.: Geology of Strand Fiord, District of Franklin. Geological Survey of Canada, Map 1301A, scale 1:250 000,
1971b.

880   Washburn, A.L.: Classification of patterned ground and review of suggested origins. Bull. Geol. Soc. Am. 67 (7), 823–865.
https://doi.org/10.1130/0016-7606(1956)67[823:COPGAR]2.0.CO;2, 1956.

Washburn, A.: Periglacial Processes and Environments. Edward Arnold, London, 1973.

885   Watson, E. and Watson, S.: Remains of pingos in the Cletwr basin, south-west Wales. GeografiskaAnnaler 56A, 213–225,
1974.

Westoby, M.J., Rounce, D.R., Shaw, T.E., Fyffe, C.L., Moore, P.L., Stewart, R.L. and Brock, B.W.: Geomorphological
evolution of a debris-covered glacier surface. Earth Surface Processes and Landforms, 45, 14, 3431–3448.
890   https://doi.org/10.1002/esp.4973, 2020.

Wolfe, S.A., Stevens, C.W., Gaanderse, A.J. and Oldenborger, G.A.: Lithalsa distribution, morphology and landscape
associations in the Great Slave Lowland, Northwest Territories, Canada. Geomorphology, 204, 302–313.
https://doi.org/10.1016/j.geomorph.2013.08.014, 2014.